Photoluminescence Properties and Analysis of Spectral Structure of Eu^{3+}-Doped SrY_2O_4

Zuoling Fu, Shihong Zhou, Yingning Yu, and Siyuan Zhang*

Laboratory of Rare Earth Chemistry and Physics, Changchun Institute of Applied Chemistry, Graduate School, Chinese Academy Sciences, Changchun 130022, China

Received: August 2, 2005; In Final Form: October 8, 2005

The aim of this work is to report on the luminescence properties of SrY_2O_4 activated by Eu^{3+} ion. Powder samples were prepared by solid-state reaction. X-ray diffraction powder data, photoluminescence, and high-resolution spectroscopy were carried out. Results revealed that the Eu^{3+} ions occupied three nonequivalent sites, with one at the Sr site, one at the Y(1) site, and another at the Y(2) site. Their spectra wavelengths for the $^7F_0-{}^5D_0$ transition are located at 578.49, 581.86, and 580.63 nm, respectively. The corresponding charge-transfer transitions are located at 248, 257, and 270 nm, respectively, which are also confirmed by theoretical analysis.

1. Introduction

Inorganic compounds doped with rare earth ions form an important class of phosphors for many luminescence applications. Phosphors doped with Eu^{3+} give rise to strong red emission and play an important role in emissive display technology, such as plasma display panel (PDP) and field emission display (FED), and in the lighting industry, such as tricolor lamps.[1−4] Sulfide-based phosphors represent one kind of important phosphor, but there are many problems with them.[5−7] When they are irradiated with an electron beam, they may cause decomposition and generate harmful gases, such as SO_2. Finally, oxide-based luminescent materials have been widely used due to their thermal and chemical stability.

SrY_2O_4 belongs to $CaFe_2O_4$-related structures, which is composed of an $R_2O_4^{2-}$ (R = rare earth metal) framework of double octahedral and alkaline earth ions residing within the framework. An activator ion (rare earth ion) could be accommodated in the $Y_2O_4^{2-}$ framework of SrY_2O_4 or within the framework depending on the size and the oxidation state of the activator ion. Eu^{3+} is especially useful and commonly utilized as a probe of the local crystal field affecting RE^{3+}. Thus it is known that the number of observed lines of the strong and easily recordable $^5D_0-{}^7F_J$ ($J = 0, 1, 2$) emission allows differentiation between Eu^{3+} in locations with different site symmetries[6,7] (in the case of SrY_2O_4 with C_s symmetry). In 2001, Xu et al. reported that SrY_2O_4:Eu^{3+} is one of the promising red phosphors for FED applications.[10] Their work shows us a new class of luminescent materials under ultraviolet (UV) excitation. In addition, Park et al. reported that the emission of SrY_2O_4:Eu^{3+} showed two nonequivalent sites of Eu^{3+} ions, which were assigned to Eu ions at Y^{3+} and Sr^{2+} sites, respectively.[11] However, these studies are not extensive, especially in luminescence of the europium dependence of the crystal structure. This paper presents results of fluorescence studies of Eu^{3+}-doped SrY_2O_4. The goal of our work was to establish and characterize the possible sites in which Eu^{3+} can be accommodated in the SrY_2O_4 lattice.

2. Experimental Section

SrY_2O_4 doped with Eu^{3+} powders were prepared by high-temperature solid-state reaction. The starting materials were $SrCO_3$ (AR), Y_2O_3 (99.99%), Eu_2O_3 (99.99%), and 0.01 H_3BO_3 as a flux. According to the nominal compositions of compounds SrY_2O_4:1% Eu, the appropriate amount of starting materials were thoroughly mixed and ground and then heated at 700 °C for 2 h. After being reground, they were calcined at 1400 °C for 2.5 h in air.

The chemical purities of these products were checked by X-ray powder diffraction (XRD) pattern at room temperature using a Rigaku D/max-IIB X-ray diffractometer with Cu Kα ($\lambda = 0.154\ 05$ nm) radiation. Photoluminescence measurements were performed on a Hitachi F-4500 fluorescence spectrophotometer equipped with a 150-W xenon lamp as the excitation source. The laser-selective excitation experiment and high-resolution emission spectra were recorded by an Acton SP-2758 spectrograph equipped with a Hamamastsu R-928 photomultiplier tube as the detector and a boxcar averager and were processed by a computer. All the measurements were performed at room temperature.

3. Results and Discussion

3.1. Crystal Structure of SrY_2O_4. SrY_2O_4 belongs to $CaFe_2O_4$-related structure; it crystallizes into an orthogonal structure with space group *Pnam* and contains four formula units for a total of 28 atoms. All of the constituent atoms occupy 4c sites according to the Wyckoff notation.[12] The orthogonal structure is constructed by an Y_2O_4-framework of double octahedra and Sr ions residing within the framework with the bicapped trigonal prismatic site. The Sr atoms are coordinated by eight oxygens and the Y atoms by six oxygens. Figure 1 shows the XRD patterns for the prepared sample SrY_2O_4:Eu^{3+}, in which all of the peaks could be indexed to the orthogonal phase of SrY_2O_4. More accurate unit-cell parameters of SrY_2O_4

* To whom correspondence should be addressed. Fax: 86-431-5698041. E-mail: syzhang@ciac.jl.cn.

10.1021/jp054273y CCC: $30.25
Published on Web 11/15/2005

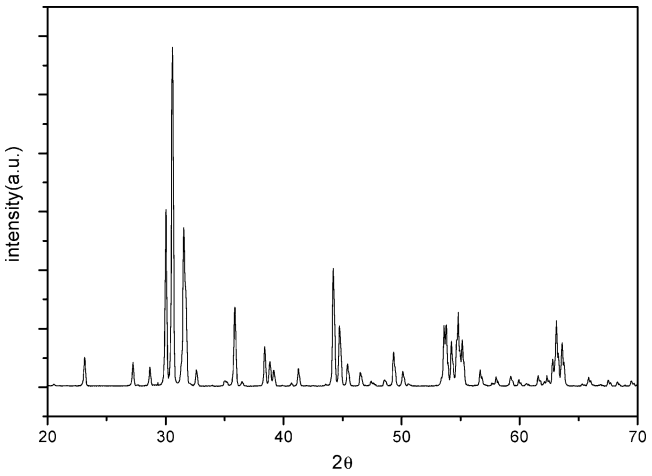

Figure 1. X-ray powder diffraction patterns of $SrY_2O_4:Eu^{3+}$ synthesized by solid- state reaction.

TABLE 1: Bond Lengths (Å) in SrY_2O_4

	bond length/Å		bond length/Å
Sr−O(1)	2.5253	Y(1)−O(2)	2.4748
Sr−O(1)	2.5253	Y(1)−O(2)	2.4748
Sr−O(2)	2.4769	Y(1)−O(3)	2.2503
Sr−O(2)	2.4769	Y(1)−O(3)	2.2503
Sr−O(3)	2.7429	Y(2)−O(1)	2.3975
Sr−O(3)	2.8327	Y(2)−O(1)	2.3975
Sr−O(4)	2.4891	Y(2)−O(3)	2.1953
Sr−O(4)	2.4891	Y(2)−O(4)	2.3642
Y(1)−O(1)	2.3712	Y(2)−O(4)	2.3502
Y(1)−O(2)	2.3422	Y(2)−O(4)	2.3502

crystal from pattern-fitting analysis software were determined, which were matched with SrY_2O_4 standard values given in JCPDS (No. 32-1272). It is indexed on an orthorhombic lattice with cell parameters $a = 10.054 \pm 0.0001$ Å, $b = 11.865 \pm 0.0001$ Å, and $c = 3.397 \pm 0.0108$ Å for $SrY_2O_4:Eu^{3+}$. The bond length of Sr−O and Y−O is shown in Table 1, which is calculated according to the crystal structure.

3.2. Photoluminescence and Excitation Spectra of $SrY_2O_4:Eu^{3+}$. The energy levels of Eu^{3+} arise from the $4f^n$configuration. In a configuration coordinate diagram these levels appear as parallel parabolas ($\Delta R = 0$), because the 4f electrons are well-shielded by $5s^25p^6$outer shells and the crystal field influence is weak. The emission arising from f−f transitions yield sharp lines in the spectra. The emission in Eu^{3+} corresponds to transitions from the excited $^5D_0$ level to the ^7F_J ($J = 0-6$) levels of the $4f^6$configuration. In addition to these emission lines, one observes often also emission from higher ^5D levels, viz., $^5D_1$, $^5D_2$, and even $^5D_3$.[13] It is well-known that the $^5D_0$ level is not split by the crystal field (because $J = 0$); the splitting of the emission transition lines yields the crystal field splitting of the ^7F_J levels. Therefore, Eu^{3+} is especially useful and commonly utilized as a probe of the local crystal field affecting RE^{3+}.

Different excitation spectra were obtained at different monitoring wavelengths of 611 and 616 nm for $SrY_2O_4:Eu^{3+}$ (Figure 2). The strong broad bands peaking at 248, 257, and 270 nm are observed, agreeing with the reported excitation of $SrY_{1.98}O_4:Eu_{0.02}$ prepared in the air.[8,10] Obviously, each excitation band could be ascribed to the charge transfer (CT) from the 2p orbital of O^{2-} to the 4f orbital of Eu^{3+}. By contrast, a small shift of the CT bands could be observed. The CT bands monitored by 611 nm were located at a shorter wavelength compared with those of 616 nm. This indicates that the broad bands near 248, 257, and 270 nm are from three different Eu sites, respectively.

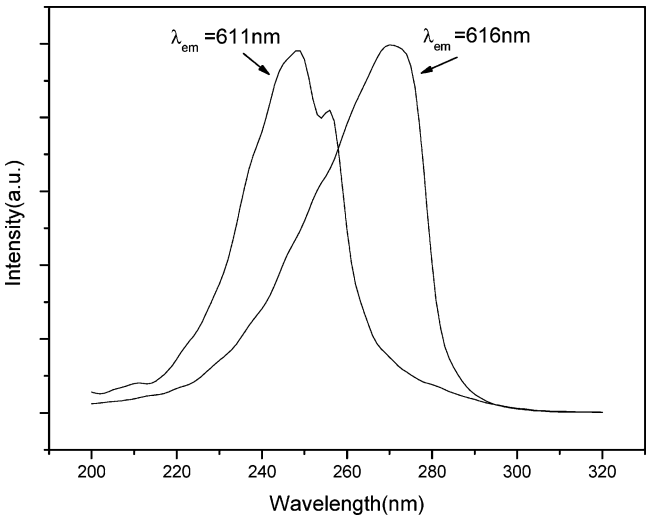

Figure 2. Excitation spectra of $SrY_2O_4:Eu^{3+}$ for the emissions at 611 and 616 nm.

Upon UV excitation, the $SrY_2O_4:Eu^{3+}$ phosphors exhibit strong red luminescence. Emission spectra of $SrY_2O_4:Eu^{3+}$ are shown in Figure 3 under excitation at 248, 257, and 270 nm in room temperature. The emission spectra not only contain the characteristic transition lines from the lowest excited $^5D_0$ level of Eu^{3+} but also those from higher energy levels ($^5D_1$, $^5D_2$, $^5D_3$) of Eu^{3+} with a weak intensity(which can be seen more clearly by enlarging the emission spectrum in the short-wavelength region). The three emission spectra of $SrY_2O_4:Eu^{3+}$ are not much different since the charge-transfer bands are wide and close to each other.

3.3. Site-Selective Fluorescence Spectra of $SrY_2O_4:Eu^{3+}$. It is well-known that the Eu^{3+} ion is sensitive to the surrounding environment, and the effect of the crystal field will cause shifts and splittings of crystal field levels. Therefore, the laser-selective excitation experiments and high-resolution emission spectra were performed on the as-synthesized sample to clarify the site occupation of Eu^{3+} doped in SrY_2O_4.

The laser-selective excitation spectra of $SrY_2O_4:Eu^{3+}$ were measured by monitoring the $^5D_0-^7F_1$ emission at 588.58 nm and displayed in Figure 4. It is well-known that the initial and final energy state involved in $^5D_0-^7F_0$ transition is nondegenerate; only a single transition is expected. The excitation spectrum, however, clearly shows three distinct $^7F_0-^5D_0$ lines at 578.49, 580.63, and 581.86 nm, which are labeled A−C, respectively. The different positions confirm the existence of at least three sites over which the Eu^{3+} dopant is distributed. Figure 5 shows the highly resolved emission spectra of SrY_2O_4: Eu^{3+} upon excitation in the A−C bands. One can observe that there is a distinct difference in three emission spectra. The emission spectra were described by the well-known $^5D_0-^7F_J$ ($J = 1-4$) line emissions of the Eu^{3+} ions. According to the relative intensity of emission, the A_1, A_2, and A_3 lines are ascribed to the $^5D_0-^7F_1$ transition of site A ($\lambda_{ex} = 578.49$ nm), the B_1, B_2, and B_3 lines are ascribed to the $^5D_0-^7F_1$ transition of site B ($\lambda_{ex} = 580.63$ nm), and the C_1, C_2, and C_3 lines are ascribed to $^5D_0-^7F_1$ transition of site C ($\lambda_{ex} = 581.86$ nm). The transitions between $^5D_0$ and ^7F_J are given in Table 2. Figure 6 is the enlarged figure of a part of Figure 5. It is clear that emission lines from three sites of $SrY_2O_4:Eu^{3+}$ could not be fully separated because three sites may possibly have energy transfer.

We know that Sr^{2+} occupies sites with C_s symmetry; Y^{3+} occupies two different octahedron sites both of C_s symmetry

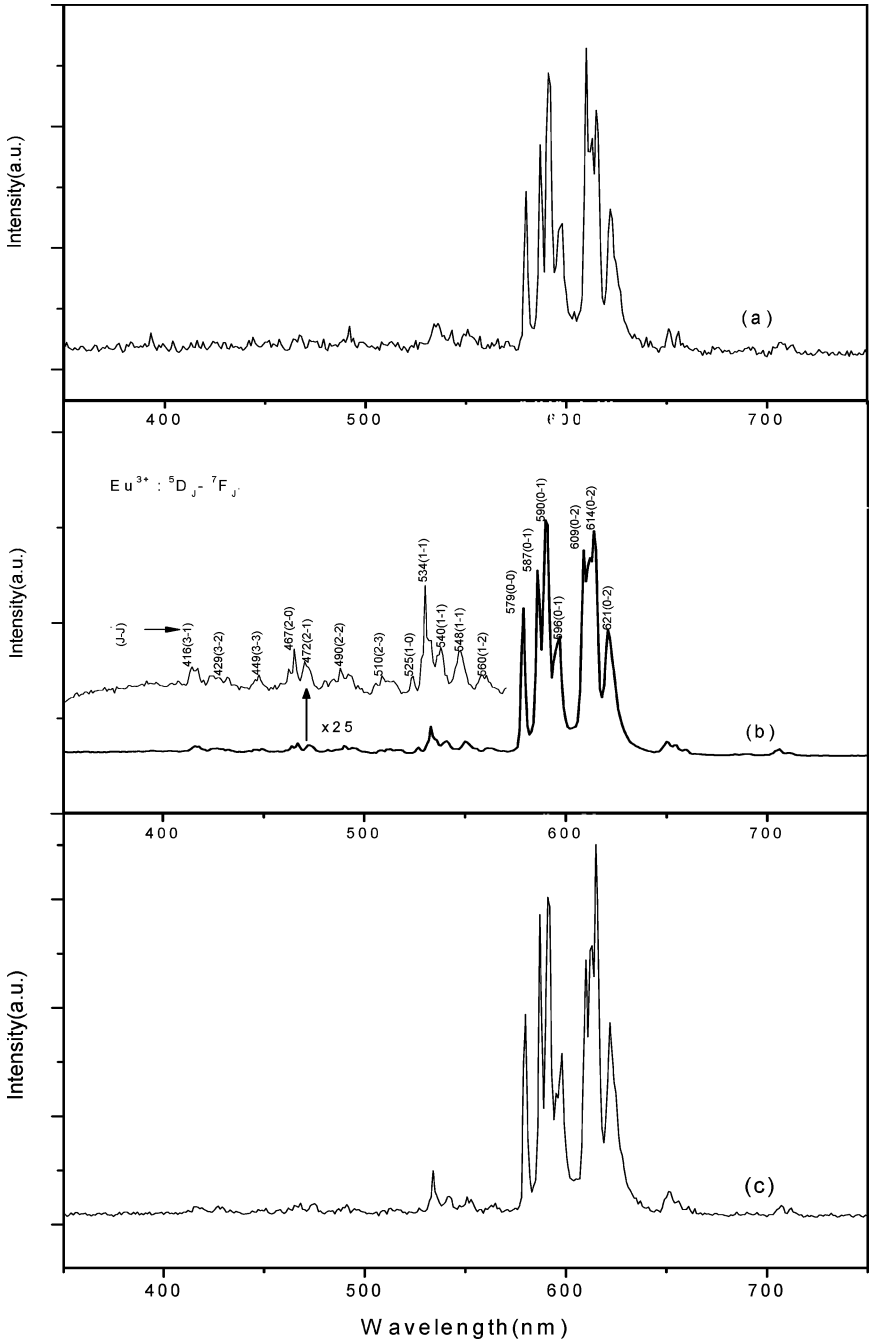

Figure 3. Emission spectrum of $SrY_2O_4:Eu^{3+}$ for the excitations at (a) 248, (b) 257, and (c) 270 nm.

with one site nearly a regular octahedron but the other much distorted.[11] Park et al. reported that the emission spectrum of $SrY_2O_4:Eu^{3+}$ showed two kinds of Eu^{3+} emissions, which could be assigned to Eu^{3+} in the Sr site and the Y site.[11] Xu et al. reported that in single-crystal fibers of $SrY_2O_4:Eu^{3+}$ there were three sites of Eu^{3+} ions giving rise to emission, corresponding to the Sr site and two nonequivalent Y sites.[10] Our recent observation in powder SrY_2O_4: Eu^{3+} reveals that there are three kinds of Eu^{3+} emissions, which should also be assignable to two nonequivalent Y sites and Sr site.

3.4. Spectral Analysis. In general, it is energetically not easy for Eu^{3+} to substitute Sr^{2+} due to the different valence states and the difference of the ion sizes between Sr^{2+} (1.260 Å, coordination number (CN) = 8) and Eu^{3+} (1.066 Å, CN = 8).In our case, the polycrystals were sintered at 1400 °C, and some trace of Eu could enter into Sr sites, which is confirmed by the site-selective excitation spectra.

A schematic energy diagram of the charge-transfer band is shown in Figure 7. It is well-known that the CT band is related to the stability of the electron of the surrounding O^{2-}; i.e., the charge-transfer transition is sensitive to the ligand environment (the bonding energy between the central ion and the ligand ions).[14] The systematic behavior in the energy needs to transfer an electron from the valence band to a trivalent lanthanide. The final state in the transition is the ground state of the divalent lanthanide ion.[15] The vertical dashed and solid arrows starting from the top of the valence band (VB) indicate the observed CT transition to the Eu^{3+} substituting Sr site (E^{Sr}_{CT}), the Y(1) site ($E^{Y(1)}_{CT}$), and the Y(2) site ($E^{Y(2)}_{CT}$), respectively. The 5d energy level of rare earth ions has closer relation to the conduction band (CB) of compound. In addition, it is considered that the energy level of the f^N configuration is approximately unchanged for Eu^{3+} replacing different cation sites since f^N are well-shielded from the surrounding electronic shell and the

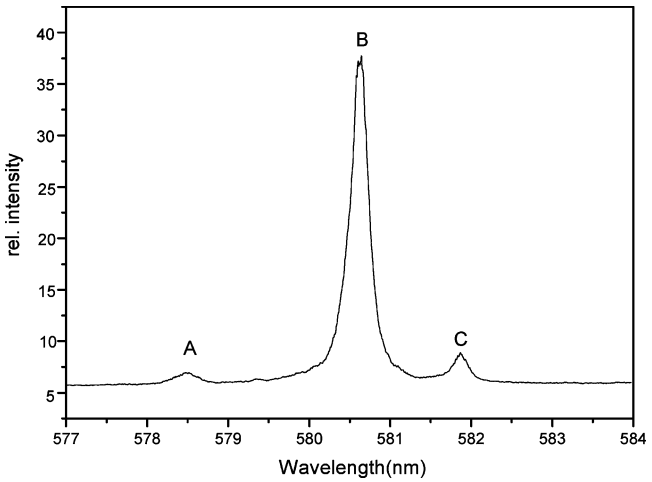

Figure 4. Excitation spectra of SrY_2O_4:Eu^{3+} measured by monitoring at 588.58 nm.

TABLE 2: Wavelength and Energy Assignment of $^5D_0-^7F_J$ ($J = 0-2$) Transitions for SrY_2O_4-Doped Eu^{3+}

transition site	*A* (nm)	*B* (nm)	*C* (nm)
$^7F_0-^5D_0$	578.49	580.63	581.86
$^5D_0-^7F_1$	586.46 (A_1)	588.64 (B_1)	591.84 (C_1)
	592.68 (A_2)	593.00 (B_2)	593.60 (C_2)
	597.38 (A_3)	599.20 (B_3)	596.98 (C_3)
$^5D_0-^7F_2$	611.38 (A_4)	611.50 (B_4)	611.44 (C_4)
	615.88 (A_5)	614.10 (B_5)	613.90 (C_5)
	619.82 (A_6)	617.04 (B_6)	617.54 (C_6)
	623.88 (A_7)	623.80 (B_7)	623.56 (C_7)
	626.20 (A_8)	626.36 (B_8)	

TABLE 3: Average Bond Length (Å), Values of Corresponding Crystal Factors, Charge-Transfer Positions, and $^5D_0-^7F_0$ Energies of Different Sites for Eu^{3+} in SrY_2O_4

	av bond length/Å	h_e	F_c	E_{CT}/nm	$^5D_0-^7F_0$/nm
Sr−O	2.5698	0.8041	0.5335	248	578.49
Y(1)−O	2.3606	1.7852	1.6883	257	581.86
Y(2)−O	2.3425	1.7549	1.7207	270	580.63

crystal field influence is weak. Finally, it is found that the energy centroid (E_c) of the 5d orbital (Eu^{3+}) and the crystal-field splitting (E_{cf}(d)) have great influence on the energy of charge transfer. According to refs 16−18, E_c is related to the environmental factor h_e, E_{cf}(d) is concerned with the environmental parameter F_c. The calculated results of h_e and F_c are listed in Table 3. It is well-known the environmental factor h_e not only can explain the center energy position of the 5d of rare earth ions but also can be define subtly the trend of the center energy levels of various crystals with the same kind of anion element according to the equation $E_c = A + Be^{-khe}$.[18] It is seen that the values of E_c increase with the decrease of h_e, which is shown in Figure 7; i.e., E_c is the highest in the Eu^{3+} replacing Sr site and the lowest in the Eu^{3+} replacing Y(1) site. In addition, it is known that when the distance of M−O (M represents cation) becomes short, F_c become large, and then the crystal splitting becomes large according to $E_{cf} = A + BF_c$.[17] In Figure 7, one can notice that if the energy centroid is higher and the crystal splitting is smaller, the CT band should be situated at higher energy (for example $E^{Sr}{}_{CT}$), which corresponds to a 248 nm excitation band in Figure 2. For two nonequivalent Y sites, the coordination number is the same, the average bond length is different, hence, h_e, and F_c are different. According to the above analyzed results, charge-transfer transitions near 257

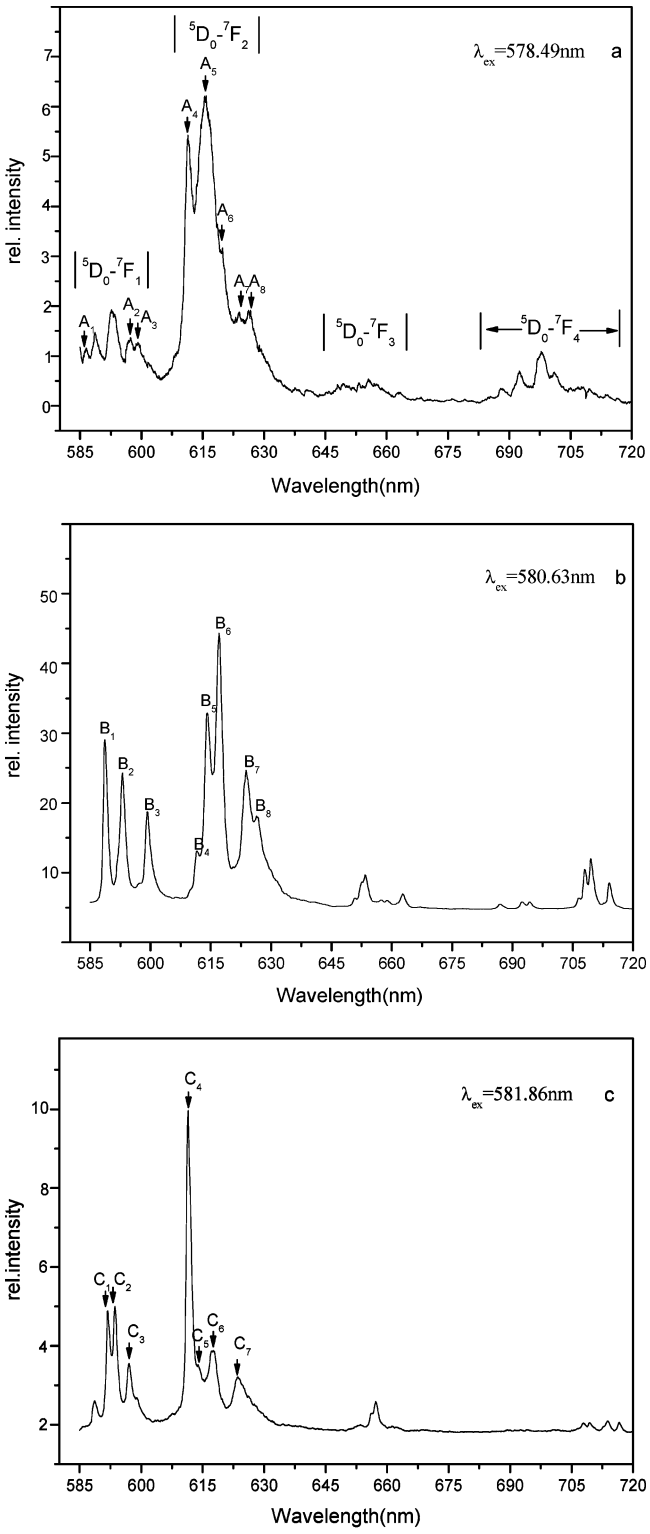

Figure 5. Highly resolved emission spectra for the excitations at 578.49 (a), 580.63 (b), and 581.86 nm (c), respectively.

and 270 nm should be assignable to the luminescence of the Eu^{3+} substituting Y(1) and Y(2) sites (see Figure 7, $E^{Y(1)}{}_{CT}$ and $E^{Y(2)}{}_{CT}$), respectively.

It is known that the $^5D_0$ to $^7F_0$ transition is both spin and electric dipole forbidden and gives rise to a weak single peak. The $^5D_0-^7F_0$ shift is directly related to the nephelauxetic effect.[19] Jørgensen[20] found that the nephelauxetic effect can be factored into the function of only a ligand and center metal $\beta = 1 - k$(center ion)h(ligand). h(ligand) is the above-mentioned h_e. In

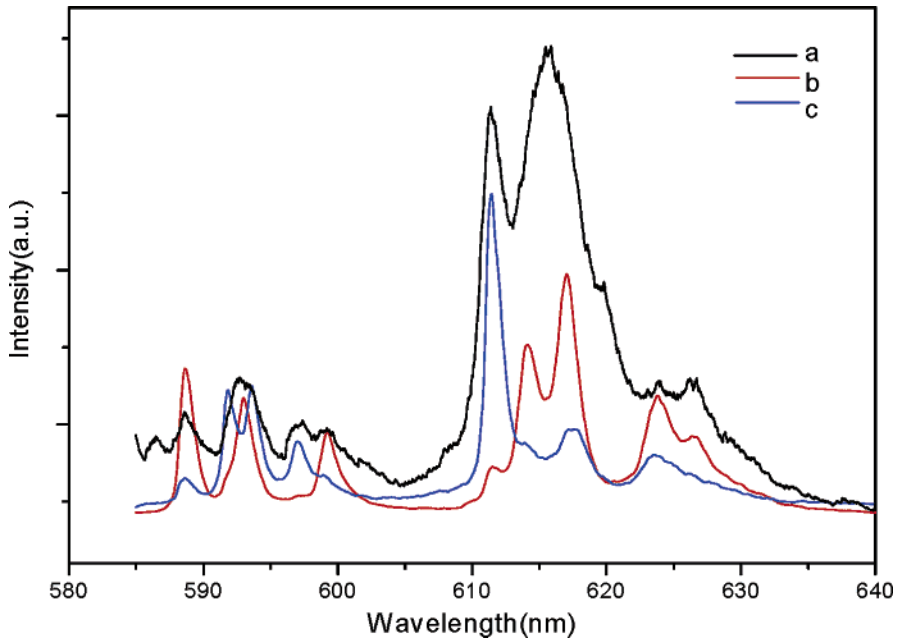

Figure 6. Enlarged figure of a part of Figure 5.

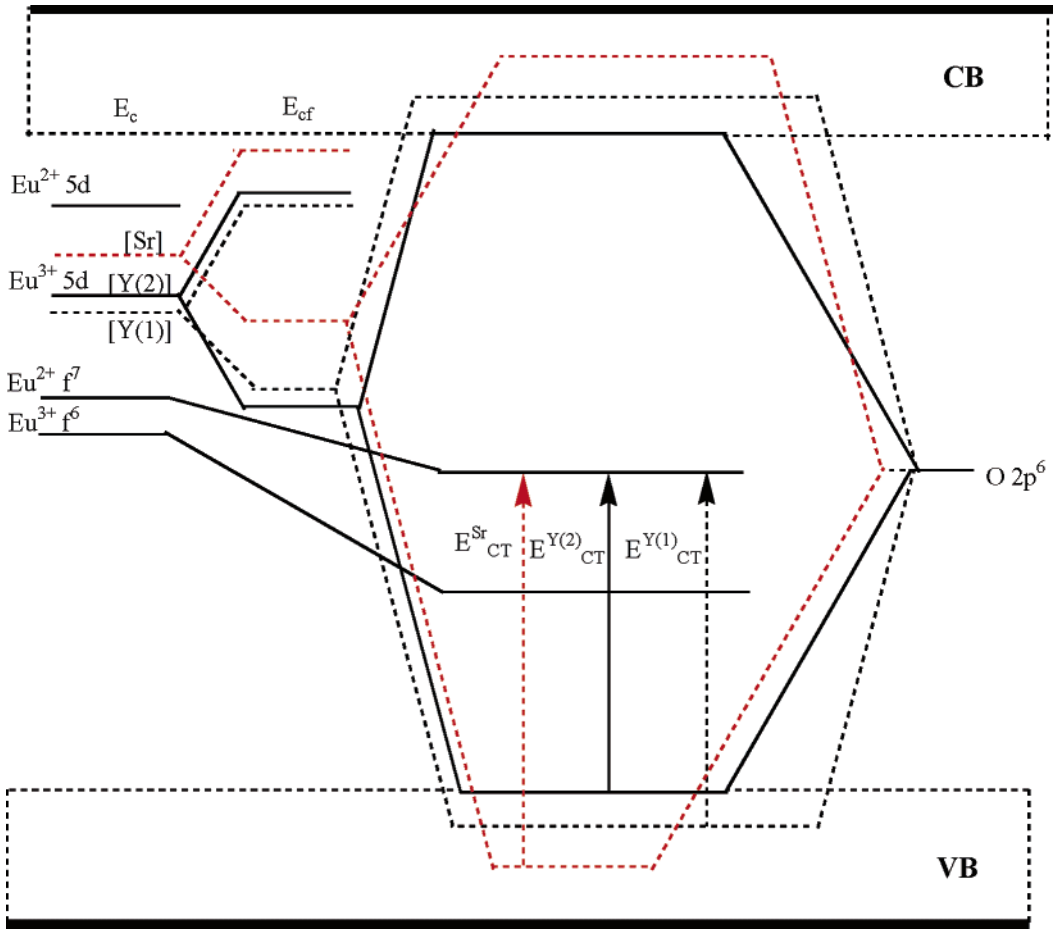

Figure 7. Schematic energy diagram of the charge-transfer band in $SrY_2O_4:Eu^{3+}$. The arrows in the figure indicate the charge-transfer transition of the Eu^{3+} substituting Sr site (E^{Sr}_{CT}), the Y(1) site ($E^{Y(1)}_{CT}$), and the Y(2) site ($E^{Y(2)}_{CT}$), respectively.

SrY_2O_4: Eu^{3+}, k is unchanged due to the same center metal Eu, decrease of h_e leads to an increase of β, and finally, the $^5D_0$ level moves to the higher energy side and closer to the free ion state (578.0 nm), which is shown in the last volume in Table 3.

4. Conclusion

SrY_2O_4: Eu^{3+} demonstrated emission from three sites of Eu^{3+} occupied in one Sr site and two Y sites, respectively, which are confirmed by the laser-selective excitation spectra and the

high-resolution emission spectra. The corresponding charge-transfer transitions for different Eu sites are located at 248, 257, and 270 nm. By combining a centroid shift and crystal-field splitting, three charge-transfer transitions should be assignable to Sr, Y(1), and Y(2) sites, respectively.

References and Notes

(1) Ronda, C. R.; Justel, T.; Nikol, H. *J. Alloys Compd.* **1998**, *275*−*277*, 669.
(2) Markku, L. *J. Alloys Compd.* **1998**, *275*−*277*, 702.
(3) Belsky, A. N.; Krupa, J. C. *Displays* **1999**, *19*, 185.
(4) Thomas, J.; Hans, N.; Cees, R. *Angew. Chem., Int. Ed.* **1998**, *37*, 3084.
(5) Souriau, J.-C.; Jiang, Y. D.; Penczek, J.; Paris, H. G.; Summers, C. J. *Mater. Sci. Eng. B* **2000**, *76*, 165.
(6) Nemec, P.; Maly, P. *J. Appl. Phys.* **2000**, *87*, 3342.
(7) Bol, A. A.; Meijerink, A. *J. Lumin.* **2000**, *87*, 315.
(8) Sinha, S. P.; Butter, E. *Mol. Phys.* **1969**, *16*, 285.
(9) Görller-Walrand, Ch.; Binnemans, K. In *Handbook on the Physics and Chemistry of Rare Earths*; Gschneidner, K. A., Jr., Eyring, L., Eds.; Elsevier: Amsterdam, 1996; Vol. 23, p 121.
(10) Xu, W. L.; Jia, W. Y.; Revira, I.; Monge, K.; Liu, H. M *J. Electrochem. Soc.* **2001**, *148*, H176.
(11) Park, S.-J.; Park, C.-H.; Yu, B.-Y.; Bae, H.-S.; Kim, C.-H.; Pyun, C.-H. *J. Electrochem. Soc.* **1999**, *146*, 3903.
(12) Müller-Buschbaum, V. H. *Z. Anorg. Allg. Chem.* **1968**, *358*, 138.
(13) Blasse, G.; Grabmaier, B. *Luminescent Materials*; Springer: Berlin, Heidelberg, New York, 1994.
(14) Blasse, G. *J. Chem. Phys.* **1966**, *45*, 2356.
(15) Dorenbos, P. *J. Lumin.* **2005**, *111*, 89.
(16) Shi, J. S.; Zhang, S. Y. *J. Phys.: Condens. Matter* **2003**, *15*, 4101.
(17) Shi, J. S.; Wu, Z. J.; Zhou, S. H.; Zhang, S. Y. *Chem. Phys. Lett.* **2003**, *380*, 245.
(18) Shi, J. S.; Zhang, S. Y. *J. Phys. Chem. B* **2004**, *108*, 18845.
(19) Blasse, G. *J. Chem. Phys.* **1966**, *45*, 2356.
(20) Jørgensen, C. K. *Progr. Inorg. Chem.* **1962**, *4*, 73.